COBEM 2023 27TH INTERNATIONAL CONGRESS OF MECHANICAL ENGENEERING

ABCM Brazilian Society of Mechanical Sciences and Engineering
27th ABCM International Congress of Mechanical Engineering
December 04-08, 2023, Florianópolis-SC, Brazil

COB-2023-488
DESIGN AND ASSEMBLY OF A MAGNETIC CIRCUIT WITH FOUR MAGNETIC FIELD REGIONS APPLIED TO A THERMOMAGNETIC MOTOR PROTOTYPE

Dalila Lima Bueno Torres[1], **dalilabt@ufmg.br**
Clara Estillac Leal Silva[1], **claraestillacls@ufmg.br**
Vinícius Souza de Jesus[1], **viniciussj3011@ufmg.br**
Gustavo Costa Mendonça[1], **Nhadefe@ufmg.br**
Higor Caldas Rios[1], **higor57@ufmg.br**
Hugo Cesar Coelho Michel[2], **hugomichel@ufmg.br**
Carmela Maria Polito Braga[2], **carmela@ufmg.br**
Paulo Vinicius Trevizoli[1], **trevizoli@demec.ufmg.br**
Marcelo Araújo Câmara[1], **marcelocamara@demec.ufmg.br**

[1] Universidade Federal de Minas Gerais, Departamento de Engenharia Mecânica - DEMEC. Av. Antônio Carlos, 6627 - Pampulha, Belo Horizonte, MG, Brasil

[2] Universidade Federal de Minas Gerais, Departamento de Engenharia Eletrônica - DELT. Av. Antônio Carlos, 6627 - Pampulha, Belo Horizonte, MG, Brasil

Abstract. *Thermomagnetic motors (TMM) are devices employed to convert low-grade thermal energy waste into mechanical energy. The generation of torque and power in a TMM relies on the variation of the magnetic phase, occurring around the Curie temperature (T_{Curie}), of a magnetic material and its interaction with an external magnetic field. This work presents the design, fabrication and assembly of a permanent magnet magnetic circuit (MC) which is part of a rotary TMM. The MC incorporates four high magnetic field regions to maximize power output. The design process involved 3D simulations in COMSOL Multiphysics, Module AC/DC, to evaluate the intensity and distribution of the magnetic field. Parameters such as the magnetic gap height and the utilization of soft magnetic materials were thoroughly investigated to enhance the magnetic field intensity and achieve greater homogeneity within the magnetic volume. The final design of the MC comprises commercially available blocks of NdFeB grade N42, arranged in a Halbach array configuration, along with ABNT 1020 steel components to enclose the magnetic circuit. During the production phase, conventional machining operations were employed, utilizing the Machine Center, to ensure the precise assembly of the MC components with minimal deviations. The quality of the production and final assembly was assessed through experimental measurements of the generated magnetic field, which were subsequently compared with the simulation results.*

Keywords: *thermomagnetic motors, magnetic circuit, desing, production, machine center*

1. INTRODUCTION

The global energy demand has experienced a rapid increase in recent decades, necessitating effective solutions to meet this growing demand. One potential approach to address this challenge involves the integration of energy harvesting devices with conventional energy systems, thereby enhancing their overall efficiency (Kishore and Priya, 2018). Specifically, energy harvesters have the capability to convert low-grade thermal waste, which is abundantly generated by industries and power plants (Forman *et al.*, 2016), into usable energy in the form of mechanical or electrical power.

Among various energy harvesting systems, thermomagnetic motors (TMM) have emerged as a promising technology for converting low-grade thermal energy, typically below 100°C, into mechanical energy (Kitanovski, 2020; **?**). The operating principle of a TMM relies on the temperature and magnetic field-dependent properties of soft magnetic materials (MM). Notably, these properties undergo significant changes around the magnetic phase transition, known as the Curie Temperature (T_{Curie}). For instance, below T_{Curie}, a soft magnetic material exhibits a high specific magnetization, whereas this magnetization tends to zero as the temperature exceeds T_{Curie}. Consequently, heating the MM causes it to transition into a non-magnetic phase, while cooling it restores the ferromagnetic state.

A TMM comprises several components, including a permanent magnet magnetic circuit (MC), a heat source and a heat sink, a heat exchanger composed of the MM, and a fluid flow system. The resultant magnetic force is proportional to the magnetic density flux gradient, the MM mass, and specific magnetization. The MC generates a high magnetic field volume. The operation begins with the MM at its ferromagnetic phase, situated in an equilibrium position within the field volume. As the MM is heated above T_{Curie}, transitioning into a non-magnetic phase, the magnetic force decreases, allowing the MM to be removed from the high-field region. Subsequently, as the MM is cooled below T_{Curie}, returning

to the ferromagnetic phase, the magnetic force increases, attracting the MM back into the magnetic volume. By repeating these processes in accordance with a thermodynamic cycle, the TMM can generate torque and power as the MM rotates or moves linearly.

Some prototypes of TMM, both linear and rotary, have been recently tested. Takahashi *et al.* (2006) designed a rotary TMM with three high magnetic field regions, utilizing a FeNiCr alloy as the MM. The device achieved a power output of 3.7 W at a rotational speed of 0.4 RPS, with the torque measured using a torquemeter. Mehmood *et al.* (2021) developed a rotary TMM with two field regions, employing Gadolinium (Gd) as MM, and reported a power output of 1 W at a speed of 220 RPM. Kaneko *et al.* (2021) designed and constructed a linear TMM with a double-C configuration in the magnetic circuit, generating two high-field regions. In this case, the system employed two magnetic heat exchangers filled with spherical particles of Gd. The cyclic variation of the magnetic phase on each heat exchanger resulted in a non-balanced magnetic force, leading to linear motion.

This work aims to present the design, production, and assembly of a permanent magnet magnetic circuit for a rotary thermomagnetic motor. The magnetic circuit is coupled with a rotor consisting of 100 Gd plates, each weighing 1.5 grams. The design of the magnetic circuit involved three-dimensional simulations in COMSOL Multiphysics, module AC/DC. These simulations enabled the evaluation of the magnetic field distribution along the rotor circumference, enabling the determination of crucial parameters such as the magnetic gap height and the selection of appropriate soft magnetic materials to guide the magnetic field lines in the magnetic circuit. These considerations were essential for maximizing the magnetic field intensity and achieving a more uniform magnetic field in volume. Following the finalization of the design, conventional machining operations were employed to fabricate all the components of the magnetic circuit, including the soft magnetic material and aluminum parts used for structural purposes. Finally, the magnetic circuit was assembled, and the magnetic flux density at the center of the magnetic volume was measured and compared with the simulation data.

2. METHODOLOGY

2.1 Magnetic circuit geometry

The initial design of the magnetic circuit took into consideration several constraints in order to meet specific requirements. These constraints were as follows:

- (i) Uniform field volume with maximum field intensity: the objective was to achieve a uniform magnetic field volume with a maximum field intensity of around 1.0 T.
- (ii) Use of commercially available permanent magnet blocks: the design aimed to utilize commercially available permanent magnet blocks to facilitate the fabrication process and ensure accessibility of the materials.
- (iii) Ease of assembly for the Gd rotor: the design needed to provide a solution for easy assembly of the Gd rotor within the magnetic circuit.
- (iv) Maximization of torque/power and continuous rotary motion: the goal was to maximize torque/power output while ensuring a continuous and smooth rotary motion of the rotor.

To address these constraints, the following solutions were proposed:

- Solution for constraints (i) and (ii): high-quality NdFeB magnets were selected to meet the desired field intensity requirements. Additionally, side concentrators were incorporated to enhance the homogeneity of the field volume, thus ensuring a more uniform distribution of magnetic flux.
- Solution for constraints (iii) and (iv): an L-configuration design with two field volumes was developed, thus the use of two independent sets establishes a total of four field volumes. This configuration facilitated the assembly of the Gd rotor, as the two sets could move freely in opposite directions. Moreover, the four high field volumes will increase torque/power output.

Fig. 1 illustrates the final design of the magnetic circuit, where the silver regions represent the magnet blocks (with arrows indicating the remanence orientation), the dark grey regions represent the aluminum structural parts, and in red are the soft magnetic material to guide the field lines. By incorporating these solutions, the magnetic circuit design successfully addressed the initial constraints, fulfilling all the initial requirements.

2.2 Materials

The magnetic circuit incorporates NdFeB permanent magnet blocks and side concentrators, utilizing commercially available dimensions. The dimensions and properties of the magnets are presented in Table 1.

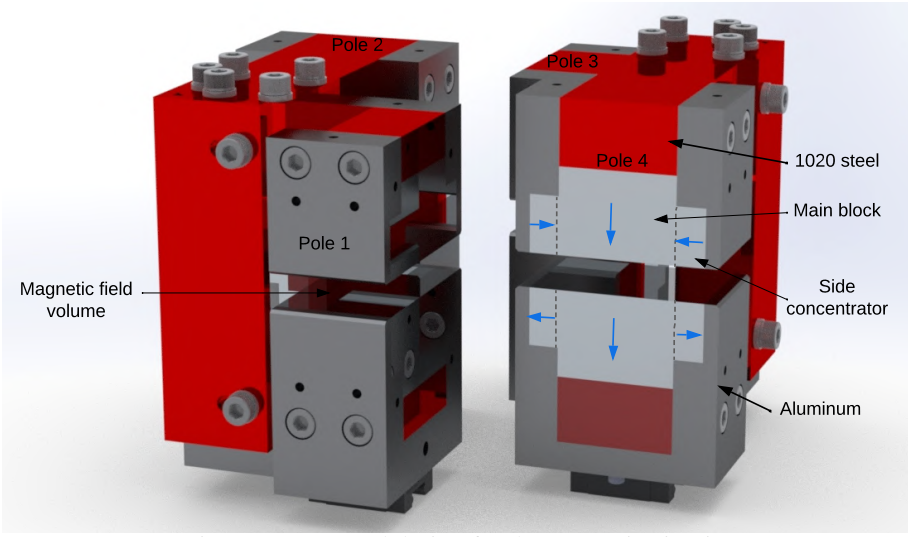

Figure 1: Proposed design for the magnetic circuit.

To select the appropriate soft ferromagnetic material, simulations were conducted using COMSOL Multiphysics (explained next) where it was included the dependence of relative permeability on magnetic field intensity. Several steel options were considered, including ABNT 1008, 1010, 1018, 1020, and 1030. The simulation results revealed minimal differences in terms of magnetic field intensity and distribution among these materials.

Considering the availability of materials from local suppliers, ABNT 1020 steel was chosen as the soft ferromagnetic material for the magnetic circuit design. Its selection ensures ease of procurement without compromising the desired magnetic field properties.

Table 1: NdFeB permanent magnets dimensions and properties.

Type	Dimensions (mm)	Grade	Remanence (T)
Main	40 x 40 x 30	N42	1,29 ∼1,33
Concentrator	40 x 20 x 10	N42	1,29 ∼1,33

2.3 COMSOL Multiphysics simulations

Three-dimensional simulations were performed using COMSOL Multiphysics, module AC/DC, no current configuration. The inputs of the simulations are the remanence values and directions of the NdFeB permanent magnets (see Table 1), the relative permeability curve of the selected soft ferromagnetic material as a function of the magnetic field, and the relative permeability of the permanent magnets. For NdFeB, the permeability is fixed 1.05 Bjørk *et al.* (2010).

The boundary conditions were set using a block of 300 x 300 mm filled with air surrounding the entire MC. The convergence criteria adopted was 3,7x10^{-4}. Additionally, it is important to mention that a mesh independence study was conducted to optimize the trade-off between simulation accuracy and computational costs, and a mesh with 250862 elements was determined to be suitable for achieving the desired results.

The main simulation output was the distribution of magnetic flux density intensity along the rotor region. The simulations considered the inclusion of the Gd rotor structure, as depicted in Fig. 1. After the convergence, the average field volume for each Gd plate in the rotor could be evaluated. This information is crucial for the further development of a mathematical model to simulate the thermomagnetic motor (TMM) as part of ongoing research. Moreover, in this study, the magnetic field distribution was analyzed along a circumference passing through the center of each magnetic field volume. This data will be compared with experimental measurements obtained at the same location.

The simulation results were then used to determine the magnetic gap height. Various values for the gap height were simulated, considering the following objectives: (a) ensuring structural integrity and allowing free rotation of the rotor, and; (b) achieving a peak magnetic field intensity of approximately 1.0 T. It was determined that a gap height of 12.0 mm strikes a suitable balance between these two objectives. The Gd plates have a height of 7.0 mm, leaving 5.0 mm of space for the rotor walls and free space between the rotor and the magnets.

2.4 Production and assembly

Conventional machining operations were employed to fabricate the components of the magnetic circuit. All fabrication processes took place in-house at the Laboratório de Usinagem e Automação from Universidade Federal de Minas Gerais. The main equipment used were the Machining Center model ROMI Discovery 560 and the band saw (Fig. 2).

The MC components, comprising both aluminum and steel parts, were produced from raw materials while respecting the selected dimensional tolerances. To ensure proper assembly and achieve the desired magnetic field intensity, cutting parameters and suitable tools were selected based on the material type of each part. High-Speed Steel (HSS) tools were employed for machining the aluminum parts, while carbide tools were utilized for working on the steel components. Appropriate cutting fluids were applied. Auxiliary tools such as bench drills, tap drills and sandpapers were employed for finishing processes.

(a) (b)

Figure 2: Equipments employed at the MC production: (a) machining center; (b) band saw

The assembly of the MC was also carried out in-house at the Laboratório de Sistemas Térmicos Emergentes – StreamLab, located at Universidade Federal de Minas Gerais. Due to the strong attractive and repulsive forces between the magnets, the assembly procedure required careful handling. Threaded bars were utilized to assist in controlling the approximation process of the permanent magnets. In order to enhance the surface roughness and remove the nickel protection layer from the permanent magnets, ensuring the best epoxy adhesion, all the bonded surfaces underwent sand filing blasting. To ensure the correct direction of the permanent magnet remanence within the MC, a Gaussmeter (model TLMP-HALL, GlobalMag) was employed (Fig. 3). The surfaces of the permanent magnets were bonded using the 3M Scotch Weld DP 460MS.

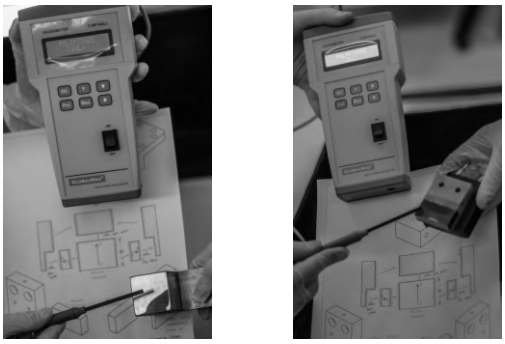

(a) (b)

Figure 3: Idenfitication of the remanence direction: (a) NdFeB main magnet; (b) side concentrator.

The assembly process of the MC involved several steps. Initially, the side concentrator magnets were bonded with the aluminum structural parts, as shown in Fig. 4, as well as the main permanent magnets were bonded with the ABNT 1020 steel parts, as in Fig.5.

Next, utilizing threaded bars, the side concentrators were coupled to the main permanent magnet structures, as showed in Fig. 6. After that, the steel parts were then placed together creating the upper and lower L-shape structures, as in Fig. 7. Finally, the upper and lower L-shape structures were joined using a triangular steel part, completing the entire assembly of the MC, as depicted in Fig. 8.

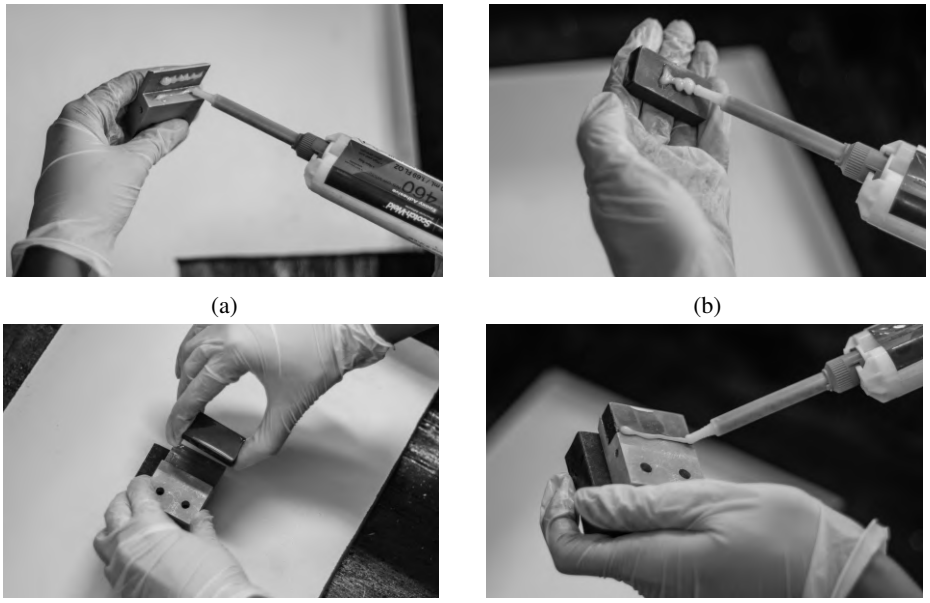

(a) (b)

(c) (d)

Figure 4: Side concentrator parts: (a) epoxy deposition at the aluminum; (b) epoxy deposition at the concentrator magnet; (c) assembly; (d) finishing process.

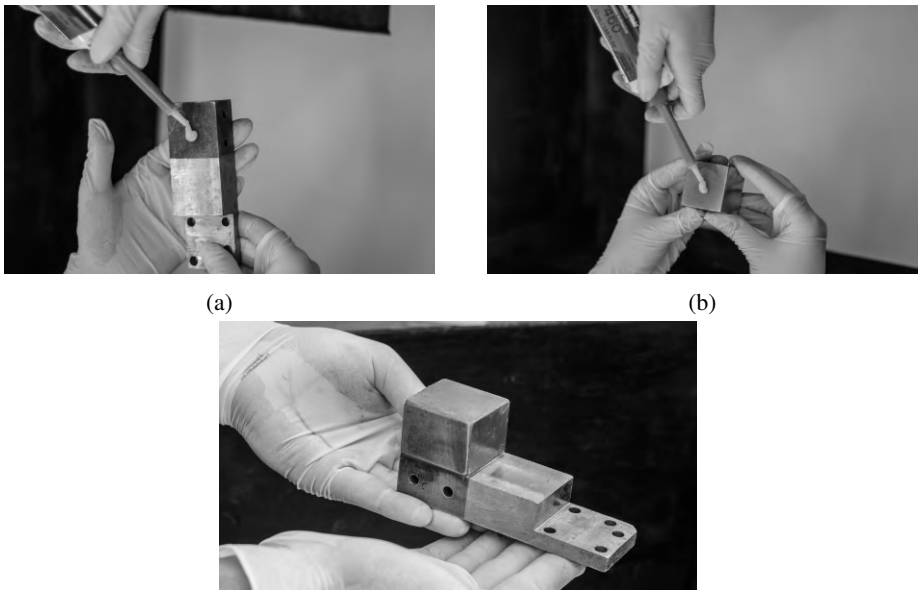

(a) (b)

(c)

Figure 5: Main magnet parts: (a) epoxy deposition at the steel; (b) epoxy deposition at the main magnet; (c) finished part.

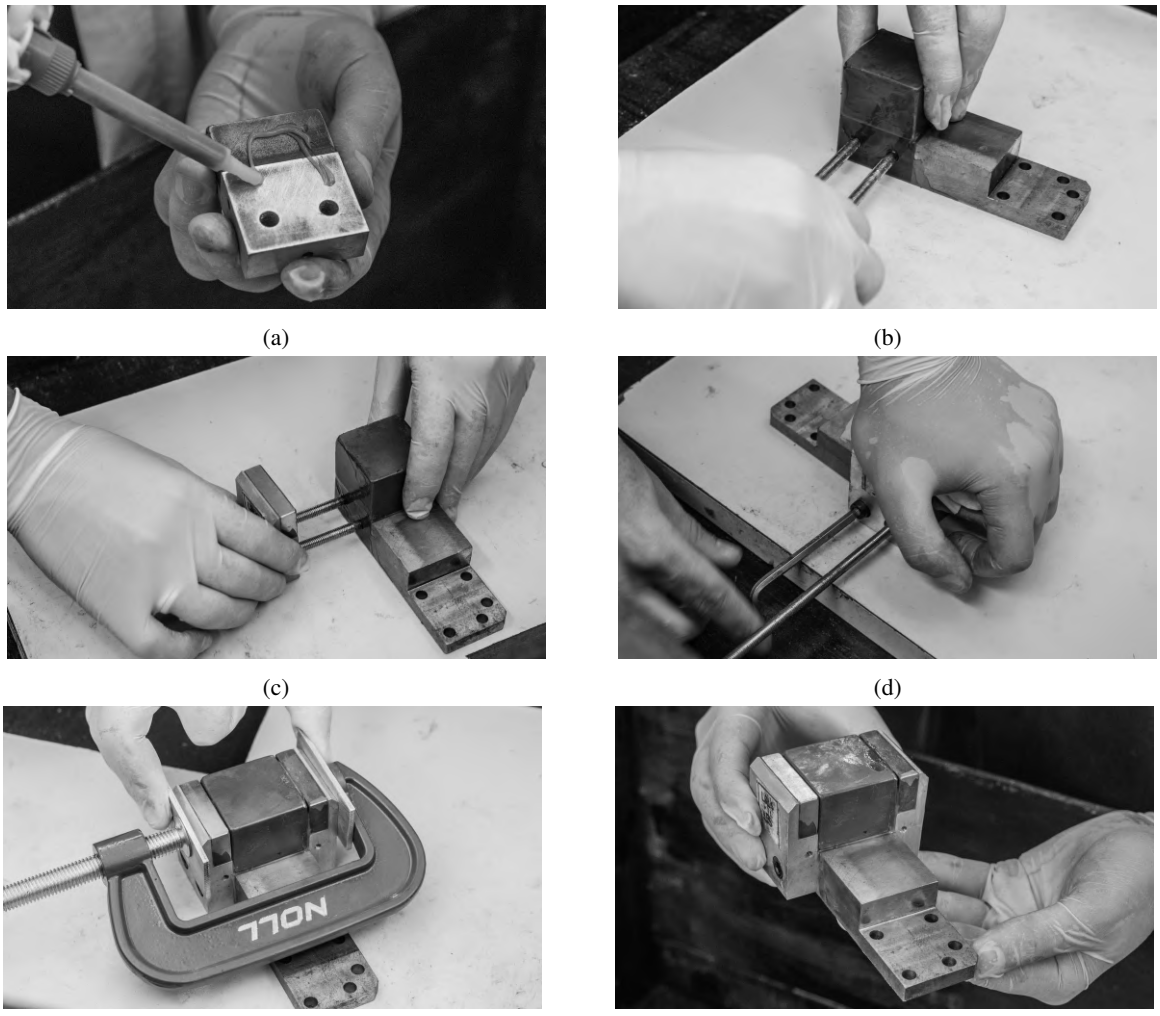

(a) (b) (c) (d) (e) (f)

Figure 6: Side concentrators and main magnets bonding: (a) epoxy deposition at the concentrator part; (b) threaded bars being used to the permanent magnet blocks approximation; (c) side concentrator approximation; (d) screw tightening; (e) magnetic pole tightening; (f) finished part.

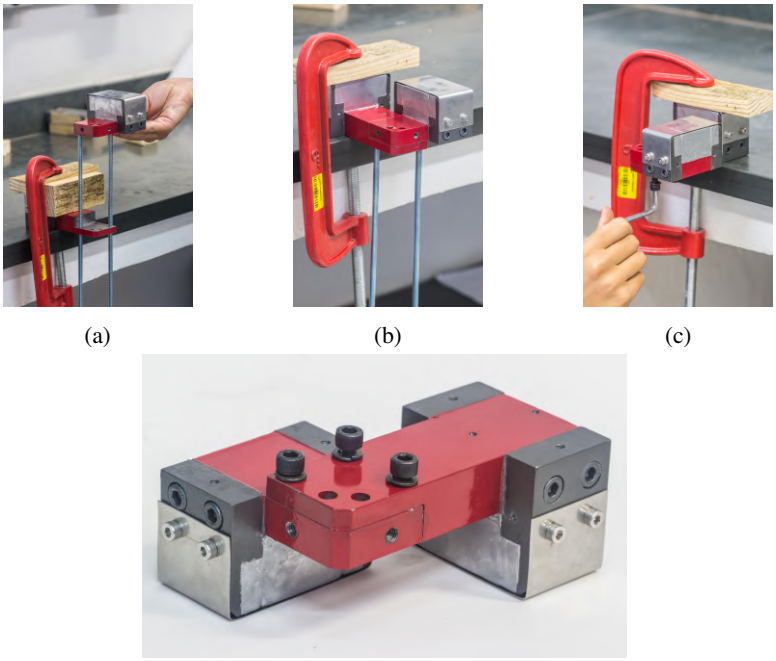

(a) (b) (c)

(d)

Figure 7: L-shape structure assembly: (a) bonded structures positioning; (b) bonded structures approximation; (c) screw tightening; (d) finished part.

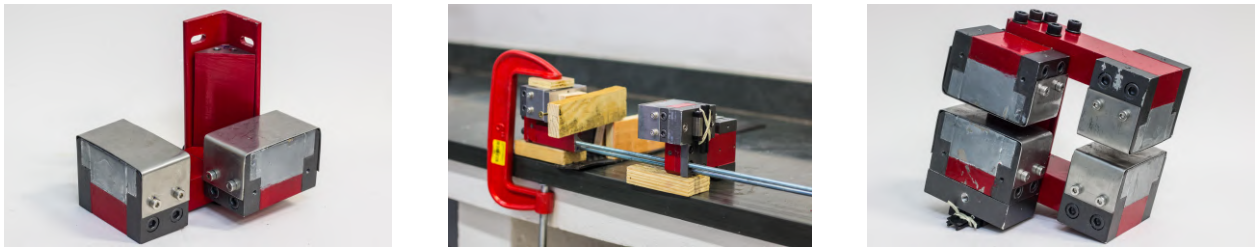

(a) (b) (c)

Figure 8: Final L-shape structure assembly: (a) triangle steel part used to connect the two L-shape structures (uper and lower); (b) Approximation of the parts; (c) Finished L-shape structure with two magnetic poles.

2.5 Experimental measurements of the magnetic flux density

After the assembly of the magnetic circuit, the magnetic flux density (B) at the center of each magnetic volume was measured experimentally using the Gaussmeter mentioned earlier. The obtained experimental data were then compared with the numerical simulation results.

To ensure accurate measurements, a specially designed tool with the same dimensions as the magnetic field volume was utilized. This tool facilitated the precise positioning of the Hall probe at the center of the volume. The x and y components of the magnetic flux density, B_x and B_y respectively, were measured. Subsequently, the magnitude of the magnetic flux density (B) was calculated using Eq. 1. The expanded uncertainty of B was estimated at 0.05 T.

$$B_{exp} = \sqrt{B_x^2 + B_y^2} \tag{1}$$

3. RESULTS AND DISCUSSION

3.1 Final Magnetic Circuit

Figure 9 illustrates the final assembly of the designed magnetic circuit. By employing the proper parameters (cutting speed, proper selecting of the tools) along the manufacturing processes, it ensures precise assembly with minimal deviations.

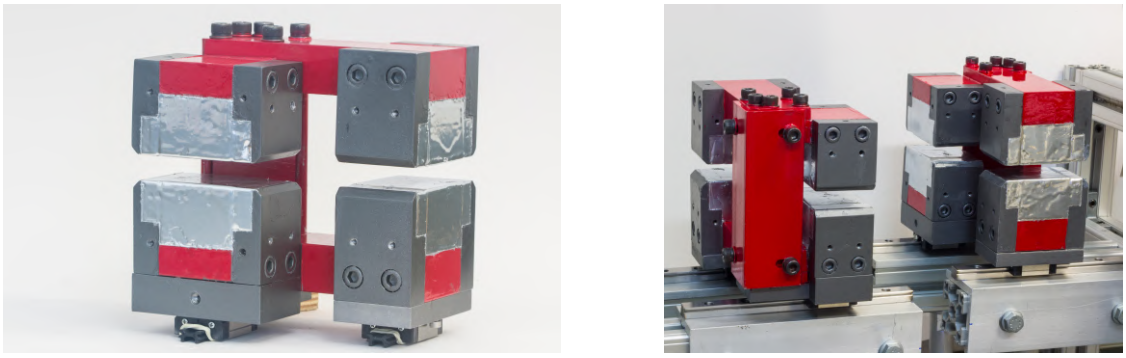

(a) (b)

Figure 9: Magnetic circuit after the final construction: (a) one of the L-shape set; (b) finished magnetic circuit.

3.2 Evaluation of the quality of the machining and assembling

The simulation results for the intensity of magnetic flux density along the circumference of the Gd rotor are presented in Figure 10. The radius of the rotor matches precisely with the center of the magnetic volume. The figure also displays the experimental field measured at the center of the volume. The maximum value of the simulated magnetic flux density is approximately 1.03 T, with a magnetic gap height of 12.0 mm.

Regarding the experimental data, each magnetic field volume generated different values: 1.053 T, 1.031 T, 1.045 T, and 1.048 T. Notably, the experimental and numerical results exhibit good agreement, with a maximum deviation of 2.1%. Therefore, it can be concluded that the production and assembly of the parts were satisfactory. However, some of the field volumes had a gap height shorter than the designed value ($<$ 12.0 mm). The smallest gap measured was approximately 10.5 mm, which leaves less space for rotor operation and explains the highest field value of 1.0526 T.

4. CONCLUSIONS

The present work focuses on the design, production, and assembly of a magnetic circuit to be used as the magnetic field source in a rotary thermomagnetic motor. Three-dimensional simulations were utilized to assist in material selection and determine the magnetic gap height, set at 12.0 mm. The simulation results indicate a maximum magnetic field value of 1.03 T, occurring at an angle of 45º from the main parallel direction of the permanent magnet.

Following the construction of the magnetic circuit, experimental measurements were taken at the center of each of the four magnetic gaps, yielding values of 1.053 T, 1.031 T, 1.045 T, and 1.048 T. The experimental results demonstrate a good agreement with the simulated values, providing confidence in the reliability of the design, production, and assembly methodology employed. The next steps of this ongoing research involve the complete characterization of the magnetic field and the final construction of the rotary thermomagnetic motor.

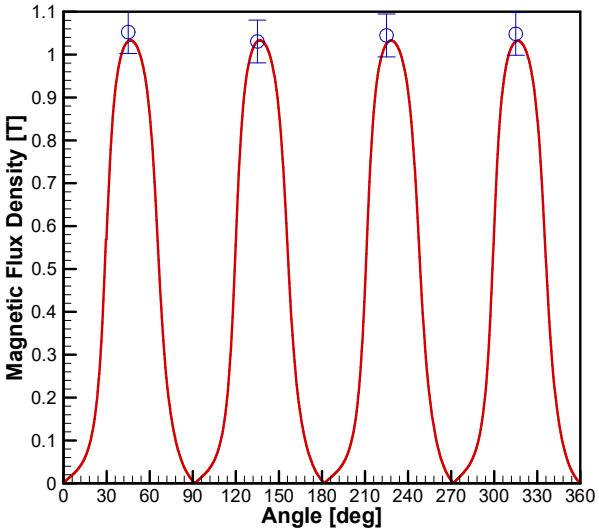

Figure 10: Magnetic flux density as a function of the angle: comparison between the simulation data and the experimental result.

ACKNOWLEDGEMENTS

The authors are grateful for the financial support from Fundação de Amparo à Pesquisa do Estado de Minas Gerais (FAPEMIG) through Grant No. APQ-00877-21 (Demanda Universal); Conselho Nacional de Desenvolvimento Científico e Tecnológico (CNPq) through Grant No. 405970/2021-8; The National Institute of Science and Technology (Refrigeration and Thermophysics) through Grant from Conselho Nacional de Desenvolvimento Científico e Tecnológico (CNPq 404023/2019-3). We also express our gratitude to Prof. Jader R. Barbosa Jr. for your help and support in regard to COMSOL Multiphysics simulations.

5. REFERENCES

Bjørk, R., Bahl, C., Smith, A. and Pryds, N., 2010. "Review and comparison of magnet designs for magnetic refrigeration". *International Journal of Refrigeration*, Vol. 33, No. 3.

Forman, C., Muritala, I.K., Pardemann, R. and Meyer, B., 2016. "Estimating the global waste heat potential". *Renewable and Sustainable Energy Reviews*, Vol. 57, pp. 1568–1579. ISSN 1364-0321. doi: https://doi.org/10.1016/j.rser.2015.12.192.

Kaneko, G., Conceição, W., Colman, F., Cocci, A., Alves, C., Pupim, G., Kubota, G., Oliveira, V. and Trevizoli, P., 2021. "Design and experimental evaluation of a linear thermomagnetic motor using gadolinium: Preliminary results". *Applied Thermal Engineering*, Vol. 186, p. 116472.

Kishore, R. and Priya, S., 2018. "A review on low-grade thermal energy harvesting: Materials, methods and devices". *Materials*, Vol. 11, No. 8. ISSN 1996-1944. doi:10.3390/ma11081433.

Kitanovski, A., 2020. "Energy applications of magnetocaloric materials". *Advanced Energy Materials*, Vol. 10. doi: https://doi.org/10.1002/aenm.201903741.

Mehmood, M.U., Kim, Y., Ahmed, R., Lee, J. and Chun, W., 2021. "Design and operation of a thermomagnetic engine for the exploitation of low-grade thermal energy". *International Journal of Energy Research*, Vol. 45, No. 10, pp. 15298–15311.

Takahashi, Y., Yamamoto, K. and Nishikawa, M., 2006. "Fundamental performance of triple magnetic circuit type cylindrical thermomagnetic engine". *Electrical Engineering in Japan*, Vol. 154, No. 4, pp. 68–74.

6. RESPONSIBILITY NOTICE

The authors are solely responsible for the printed material included in this paper.